Modeling of tsunami generation by an underwater landslide in a 3D-NWT*

Stéphan T. Grilli [1] *and Philip Watts* [2]

1. Department of Ocean Engineering, University of Rhode Island, Narragansett, RI 02882, USA

2. Applied Fluids Engineering, Inc., Private Mail Box #237, 5710 E. 7th Street, Long Beach, CA 90803, USA

ABSTRACT

An existing three-dimensional (3D) Numerical Wave Tank (NWT) solving fully nonlinear potential flow theory with a higher-order Boundary Element Method (BEM) is modified to simulate tsunami generation by underwater landslides. New features are added to the NWT to model underwater landslide geometry and motion and specify corresponding boundary conditions in the BEM model. Also, new snake absorbing piston boundaries are implemented to remove reflection from the onshore and offshore boundaries of the NWT. Two cases of tsunami generation are presented and results of the first one are validated using experimental results. Numerical accuracy is examined and found to be excellent in both cases.

KEYWORDS : tsunamis, landslides, numerical wave tank, nonlinear wave transformations, boundary element method.

INTRODUCTION

Tsunamis generated by underwater landslides appear to be one of the major coastal hazards for moderate earthquakes (e.g., Tappin *et al.*, 1999, 2000). Whereas tsunamis generated by direct coseismic displacement are usually relatively small in height (which correlates with moment magnitude), landslide tsunamis are only limited in height by the landslide vertical displacement (Murty, 1979; Watts, 1997, 1998). Since underwater landslides are usually triggered on the continental slope, such displacements may reach several thousand meters, and thus produce huge tsunamis which offer little time for warning due to their proximity to shore (Grilli and Watts, 1999; Watts, 2000). There is evidence, for instance, that the large tsunami originating near Unimak Island along the Aleutian Trench in 1946 was caused by a giant $\approx$200 km^3 underwater landslide triggered by a magnitude M_s =7.1 earthquake (Fryer *et al.*, 2001). The landslide headscarp was on the shallow continental shelf in 150 m water depth, and the landslide mass moved down a 4° mean slope, to the 4,000 m deep Aleutian Terrace, where parts of it apparently stopped. Local runup for this tsunami reached 35 m above sea level at Scotch Cap lighthouse.

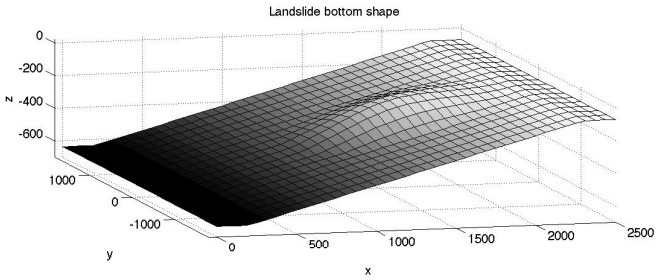

Fig. 1 : Example of underwater landslide shape on a planar slope in the 3D-NWT. For $\theta = 15°$, $B = 1,000$ m, $W = 1,168$ m, $T = 103$ m, $d = 156$ m, $x_\ell = 1,592.7$ m, $\varepsilon = 0.25$ (Eqs. (16)-(21)), $h_o = 635.8$ m, $x_o = 0$, $d_o = 200$ m, $l_o = 2,300$ m, $h_1 = 73.12$ m (Fig. 2).

Predicting landslide tsunamis requires complex numerical models which must accurately represent both landslide and bottom geometry, and the nonlinear interactions between landslide motion and surface wave field. Such a model has been demonstrated by Grilli and Watts (1999), in their implementation of a two-dimensional (2D) Numerical Wave Tank (NWT) for underwater landslides. Reviews of the literature to date regarding tsunamis generated by underwater landslides and their numerical modeling can be found in the latter paper and in Watts *et al.* (2000).

Here, we describe the current implementation and simulation of tsunami generation by underwater landslides in the three-dimensional (3D) NWT developed by Grilli *et al.* (2000, 2001). Fully nonlinear potential flow equations are solved in this NWT, based on a higher-order Boundary El-

*To appear in *Proc. ISOPE 2001 Conf.* (Stavanger, Norway)

ement Method and an explicit time stepping scheme. Wave overturning can be modeled if it occurs in the computations. Grilli *et al.* validated their 3D-NWT for solitary wave shoaling and breaking over slopes, by comparing results both to experiments and to an earlier numerical solution. The agreement was excellent and it was found that almost arbitrary accuracy could be obtained from precise initial and boundary conditions, through careful discretization of the simulation domain.

Various improvements to the NWT were made to efficiently simulate underwater landslides. Open boundaries were implemented and validated for solitary wave propagation over constant depth, which extend to 3D the piston-like boundary condition used by Clément (1996) and Grilli and Horrillo (1997). The landslide shape and kinematics were modeled on a way similar to Grilli and Watts' (1999) 2D model, by assuming a smooth initial shape for the landslide, moving over a planar slope (e.g., Fig. 1).

Once the relationship of result accuracy versus spatio-temporal discretization is assessed, numerical experiments can be performed in the 3D-NWT for specified initial and boundary conditions, herein for underwater landslides. This is an important point : the exact nature of wave generation is both known and controlled. Different motions of the same submerged body can produce very different waves, and such wave differences can be directly related to the input parameters of the motion. This is the basis of the wavemaker formalism introduced by Watts (1998, 2000). NWTs enable many experimental outputs to be obtained with minimal error, and in virtually no setup time. While output choices include free surface profiles, numerical wave gages, runup, etc. . . , as done in earlier 2D studies (Grilli and Watts, 1999), we usually represent results of the 3D-NWT by a characteristic wave amplitude measured above the initial landslide position, at the location of maximum landslide thickness (defined at horizontal location $(x_\ell, 0)$ in the following; Fig. 2). Our characteristic wave amplitude is an implicit function of the underwater landslide shape and motion input parameters.

THE NUMERICAL WAVE TANK

Governing equations and boundary conditions

Equations for fully nonlinear potential flows with a free surface are summarized below. The velocity potential is defined as $\phi(\mathbf{x}, t)$ and describes inviscid irrotational 3D flows in Cartesian coordinates $\mathbf{x} = (x, y, z)$, with z the vertical upward direction (and $z = 0$ at the undisturbed free surface; Fig. 2). The velocity is defined by, $\mathbf{u} = \nabla\phi = (u, v, w)$.

Continuity in the fluid domain $\Omega(t)$, with boundary $\Gamma(t)$, is a Laplace's equation for the potential,

$$\nabla^2\phi = 0 \qquad \text{in } \Omega(t) \qquad (1)$$

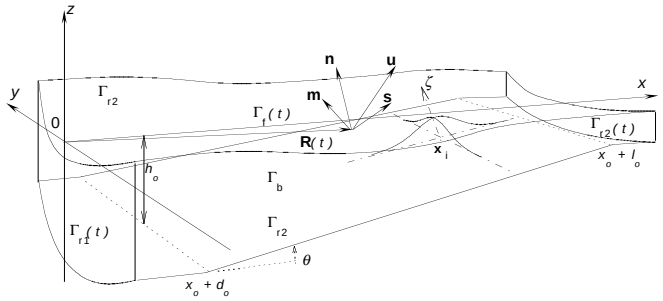

Fig. 2 : Sketch of NWT used for landslide tsunami modeling. The landslide is moving in the negative x direction on bottom boundary Γ_b. Snake absorbing pistons are modeled on boundaries $\Gamma_{r1}(t)$ and $\Gamma_{r2}(t)$. The bottom is of constant depth $h = h_o$ in deep water and sloping from $x = x_o + d_o$, with slope θ, to $x_o + l_o$ where a shelf of depth h_1 of initial length l_1 is located. The landslide is located on the slope with its axis intersecting it at point $\mathbf{x}_i$ (see also Fig. 1). Tangential vectors at point $\mathbf{R}(t)$ on the free surface $\Gamma_f(t)$ are defined as $(\mathbf{s}, \mathbf{m})$ and outward normal vector as $\mathbf{n}$.

The 3D free space Green's function for Eq. (1) is defined as,

$$G = \frac{1}{4\pi\, r} \quad \text{with} \quad \frac{\partial G}{\partial n} = -\frac{1}{4\pi}\,\frac{\mathbf{r}\cdot\mathbf{n}}{r^3}\,, \qquad (2)$$

with $\mathbf{r} = \mathbf{x} - \mathbf{x}_l$ and $r = \mid \mathbf{r} \mid$, where $\mathbf{x}$ and $\mathbf{x}_l = (x_l, y_l, z_l)$ are points on boundary Γ, and $\mathbf{n}$ is the outward unit vector normal to the boundary at point $\mathbf{x}$.

Green's second identity transforms Eq. (1) into the Boundary Integral Equation (BIE),

$$\alpha_l\,\phi_l = \int_\Gamma \left\{ \frac{\partial\phi}{\partial n}(\mathbf{x})\, G(\mathbf{x}, \mathbf{x}_l) - \phi(\mathbf{x})\,\frac{\partial G}{\partial n}(\mathbf{x}, \mathbf{x}_l) \right\} \mathrm{d}\Gamma \qquad (3)$$

in which $\alpha_l = \alpha(\mathbf{x}_l) = \theta_l/(4\pi)$, with θ_l the exterior solid angle made by the boundary at point $\mathbf{x}_l$ (i.e., 2π for a smooth boundary).

The boundary is divided into various sections, with different boundary conditions (Fig. 2). On the free surface $\Gamma_f(t)$, ϕ satisfies the nonlinear kinematic and dynamic boundary conditions,

$$\frac{D\,\mathbf{R}}{D\,t} = \mathbf{u} = \nabla\phi \qquad \text{on } \Gamma_f(t) \qquad (4)$$

$$\frac{D\,\phi}{D\,t} = -gz + \frac{1}{2}\,\nabla\phi\cdot\nabla\phi - \frac{p_a}{\rho_w} \qquad \text{on } \Gamma_f(t) \qquad (5)$$

respectively, with $\mathbf{R}$ the position vector of a free surface fluid particle, g the acceleration due to gravity, p_a the atmospheric pressure, ρ_w the fluid density, and D/Dt the material derivative.

Various methods can be used for wave generation in the NWT. Here, tsunamis are generated on the free surface due

to a specified landslide motion $\mathbf{x}_\ell(t)$ on the bottom boundary Γ_b (Fig. 1). We have,

$$\overline{\mathbf{x}} = \mathbf{x}_\ell \;\; ; \;\; \overline{\frac{\partial \phi}{\partial n}} = \mathbf{u}_\ell \cdot \mathbf{n} = \frac{\mathrm{d}\mathbf{x}_\ell}{\mathrm{d}\,t} \cdot \mathbf{n} \qquad \text{on } \Gamma_b(t) \qquad (6)$$

where overlines denote specified values, and the time derivative follows the landslide motion. See below for details.

Along stationary parts of the boundary, such as some lateral parts of Γ_{r2}, a no-flow condition is prescribed as,

$$\overline{\frac{\partial \phi}{\partial n}} = 0 \qquad \text{on } \Gamma_{r2} \qquad (7)$$

Assuming the landslide motion is in the negative x direction, actively absorbing boundary conditions are specified at both extremities of the NWT, initially at $x = x_o$ and $x_o + l_o + l_1$ (Fig. 2). These are modeled as pressure sensitive "snake" absorbing piston wavemakers. The piston normal velocity is specified as,

$$\overline{\frac{\partial \phi}{\partial n}} = u_{ap}(\sigma, t) \qquad \text{on } \Gamma_{r2}(t), \text{ with,} \qquad (8)$$

$$u_{ap}(\sigma, t) = \frac{1}{\rho_w h_o \sqrt{g h_o}} \int_{-h_o}^{\eta_{ap}(\sigma,t)} p_D(\sigma, z, t)\, \mathrm{d}z \qquad (9)$$

calculated at the curvilinear abscissa σ, horizontally measured along the piston, where η_{ap} is the surface elevation at the piston and $p_D = -\rho_w \{\frac{\partial \phi}{\partial t} + \frac{1}{2} \nabla\phi \cdot \nabla\phi\}$ denotes the dynamic pressure. The integral in Eq. (9) represents the horizontal hydrodynamic force $F_D(\sigma, t)$ acting on the piston at time t, as a function of σ.

For well-posed problems, we have, $\Gamma \equiv \Gamma_f \cup \Gamma_b \cup \Gamma_{r1} \cup \Gamma_{r2}$.

Time integration

Free surface boundary conditions (4) and (5) are integrated at time t to establish both the new position and the boundary conditions on the free surface $\Gamma_f(t)$ at a subsequent time $(t + \Delta t)$ (with Δt a varying time step).

To do so, second-order explicit Taylor series expansions are used to express both the new position $\mathbf{R}(t + \Delta t)$ and the potential $\phi(\mathbf{R}(t + \Delta t))$ on the free surface, in a MEL formulation (see Grilli *et al.*, 2001, for details). First-order coefficients in the Taylor series are given by Eqs. (4) and (5), which require calculating $(\phi, \frac{\partial \phi}{\partial n})$ on the free surface. This is done by solving Eq. (3) at time t, with boundary conditions (6) to (9). Second-order coefficients are obtained from the material derivative of Eqs. (4) and (5), which requires also calculating $(\frac{\partial \phi}{\partial t}, \frac{\partial^2 \phi}{\partial t \partial n})$ at time t. This is done by solving a BIE similar to Eq. (3) for the $\frac{\partial \phi}{\partial t}$ field. The free surface boundary condition for this second BIE is obtained from Bernoulli Eq. (4), after solution of the first BIE for ϕ as,

$$\overline{\frac{\partial \phi}{\partial t}} = -gz - \frac{1}{2} \nabla\phi \cdot \nabla\phi - \frac{p_a}{\rho_w} \qquad \text{on } \Gamma_f(t) \qquad (10)$$

For wave generation by an underwater landslide, Eq. (6) gives,

$$\overline{\frac{\partial^2 \phi}{\partial t \partial n}} = \frac{\partial (\mathbf{u}_\ell \cdot \mathbf{n})}{\partial t} \qquad \text{on } \Gamma_b(t) \qquad (11)$$

and for stationary boundaries,

$$\overline{\frac{\partial^2 \phi}{\partial t \partial n}} = 0 \qquad \text{on } \Gamma_{r2} \qquad (12)$$

For the absorbing conditions we have, from Eq. (9),

$$\overline{\frac{\partial^2 \phi}{\partial t \partial n}} = \frac{\partial u_{ap}(\sigma, t)}{\partial t} \qquad \text{on } \Gamma_{r2}(t) \qquad (13)$$

The adaptive time step Δt in the Taylor series is calculated at each time from the minimum distance between nodes on the free surface and a constant mesh Courant number $\mathcal{C}_o \simeq 0.5$ (see Grilli *et al.*, 2001, for details).

Discretization

The spatial discretization follows that of Grilli *et al.*'s (2001) model. All details can be found in the latter reference.

The BIEs for ϕ and $\frac{\partial \phi}{\partial t}$ are solved by a Boundary Element Method (BEM). The boundary is discretized into collocation nodes and cubic sliding boundary elements, based on polynomial shape functions. These are expressed over 4 by 4 node reference elements, of which only one 4-node quadrilateral is used as the boundary element. Curvilinear changes of variables are used for expressing boundary integrals over reference elements and deriving dicretized equations. Discretized boundary integrals, both regular and singular, are calculated for each collocation node by numerical integration. Double and triple nodes and edges are used to specify BIEs at intersecting parts of the boundary. The algebraic system is solved in the present applications with a direct elimination method.

Tangential derivatives, e.g., needed in the Taylor series, are calculated on the boundary in a local curvilinear coordinate system $(\mathbf{s}, \mathbf{m}, \mathbf{n})$ defined at each boundary node (Fig. 2), with $\mathbf{s} = \mathbf{x}_s$, $\mathbf{m} = \mathbf{x}_m$, and $\mathbf{n} = \mathbf{s} \times \mathbf{m}$ (subscripts indicate partial derivatives). Derivatives of the geometry and field variables in tangential directions $\mathbf{s}$ and $\mathbf{m}$ are computed, by defining, around each node, a local 5 node by 5 node, 4th-order, sliding element (see Grilli *et al.*, 2001, for details).

Because of the difference between partial, material, and time derivatives following a boundary motion, it is necessary to further develop equations such as (11) and (13). For a landslide, we find, from Eq. (11) with Eq. (6) for ϕ_n,

$$\begin{aligned} \overline{\frac{\partial^2 \phi}{\partial t \partial n}} \;\; = \;\; & (\frac{\mathrm{d}\mathbf{u}_\ell}{\mathrm{d}t} \cdot \mathbf{n}) + (\mathbf{u}_\ell \cdot \frac{\mathrm{d}\mathbf{n}}{\mathrm{d}t}) - \phi_n \phi_{nn} \\ & - (\mathbf{u}_\ell \cdot \mathbf{s})\, \phi_{ns} - (\mathbf{u}_\ell \cdot \mathbf{m})\, \phi_{nm} \end{aligned} \qquad (14)$$

with,

$$\begin{aligned} \phi_{nn} \;\; = \;\; & -\phi_{ss} - \phi_{mm} + \phi_s \{\mathbf{x}_{ss} \cdot \mathbf{s} - \mathbf{x}_{sm} \cdot \mathbf{m}\} \\ & + \phi_m \{\mathbf{x}_{mm} \cdot \mathbf{m} - \mathbf{x}_{sm} \cdot \mathbf{s}\} \\ & + \phi_n \{\mathbf{x}_{ss} \cdot \mathbf{n} + \mathbf{x}_{mm} \cdot \mathbf{n}\} \end{aligned} \qquad (15)$$

where, $\mathrm{d}\mathbf{u}_\ell/\mathrm{d}t = \dot{\mathbf{u}}_\ell$ denotes the absolute landslide acceleration, and $\mathrm{d}\mathbf{n}/\mathrm{d}t = \dot{\Omega}\mathbf{j} \times \mathbf{n}$ denotes rotation with angular velocity $\dot{\Omega}(y,t)$ around axis y of unit direction $\mathbf{j}$. [Note, upper dots indicate time derivatives $\mathrm{d}/\mathrm{d}t$ following the landslide motion.]

A similar expression is derived from Eq. (13), for a snake absorbing piston. See Brandini and Grilli (2001) (in these Proceedings) for details.

Landslide geometry

Underwater landslides are represented by a fully submerged smooth sediment mound of density ρ_ℓ sitting over a planar slope of angle θ (Figs. 1 and 2). The landslide has maximum thickness T (measured perpendicularly to the slope). The middle of the landslide surface is located in depth d at a distance x_ℓ along the x-axis. Semi-ellipses were used to represent the geometry of landslide cross-sections in Grilli and Watts' 2D model, and were moved downslope according to specified landslide kinematics (see below). A semi-ellipse introduced sharp corners at the intersection between the landslide and the planar slope, and it also required regridding the planar slope nodes both behind and ahead of the landslide at each time step. Here, $T\,\mathrm{sech}^2(k\,r_\ell)$ curves, truncated where they reach an elevation less than $\varepsilon\,T$, are used to represent the landslide geometry, in polar coordinates (r_ℓ, φ_ℓ) defined within the slope and centered on the landslide axis at point $\mathbf{x}_i$ (Fig. 2). This provides for a smoother bottom geometry and eliminates the need to round corners. Also, no bottom regridding is performed and the landslide is treated as a "wave" of bottom elevation moving downslope. The landslide footprint on the bottom slope is defined as an ellipse of major axis b (in the x direction) and minor axis w (in the y direction). These dimensions are functions of specified characteristic dimensions (B, W) which, with T, define the landslide volume. We assume, for the sake of simplicity and comparison with other work, the landslide volume is identical to that of the semi-ellipsoid (B, W, T),

$$V_\ell = \frac{1}{6}\,\pi\,T\,B\,W \tag{16}$$

In general, the landslide geometry is defined by its elevation perpendicular to the slope, as (Fig. 2),

$$\zeta = \frac{T}{1-\varepsilon}\left\{\mathrm{sech}^2(k\,r_\ell) - \varepsilon\right\} \tag{17}$$

where $r_\ell = \sqrt{(x-x_i)^2 + y^2}$, with (Fig. 2),

$$\begin{aligned} x_i &= x_\ell + T\,\sin\theta \\ x_\ell &= d_o + \frac{1}{\tan\theta}\left\{h_o - d - \frac{T}{\cos\theta}\right\} \end{aligned} \tag{18}$$

the landslide axis abscissa on the slope (assuming $y_i = 0$), and abscissa of minimum depth d, respectively. Landslide geometry is truncated along a planar ellipse defined as,

$$r_{\ell o}(\varphi_\ell, b, R) = \frac{b}{2}\left\{\cos^2\varphi_\ell + R^2\,\sin^2\varphi_\ell\right\}^{-\frac{1}{2}} \tag{19}$$

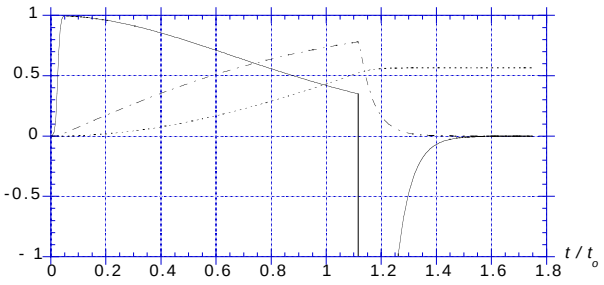

Fig. 3 : Nondimensional landslide kinematics modeled as a function of dimensionless time : S/S_o (- - - - -); $\dot{S}/u_t$ (— - —); $\ddot{S}/a_o$. The acceleration ramp-up has a duration $t_o/20$. The sharp deceleration starts at $t = 1.15t_o$. [Note, the minimum acceleration was truncated for figure scaling purpose.]

with the ratio $R = b/w = B/W$ and,

$$k(\varepsilon, \varphi_\ell, b, R) = \frac{1}{r_{\ell o}}\,\mathrm{acosh}\frac{1}{\sqrt{\varepsilon}} \tag{20}$$

Equating the landslide volume to V_ℓ in Eq. (16), we eventually find,

$$b = B\,\frac{C\sqrt{1-\varepsilon}}{\left\{3\left[\sqrt{1-\varepsilon}\,C - \ln\frac{1}{\sqrt{\varepsilon}} - \frac{\varepsilon}{2}\,C^2\right]\right\}^{\frac{1}{2}}} \tag{21}$$

where $C(\varepsilon) = k\,r_{\ell o} = \mathrm{acosh}(1/\sqrt{\varepsilon})$, and $w = b/R$. In Eq. (21), the term multiplying B is only a function of ε. For $\varepsilon = 0.25$, for instance, we find $C = 1.317$ and $b = 1.371B$. The initial landslide geometry $\mathbf{x}_\ell(0)$ is defined using Eqs. (17) to (21). An example is given in Fig. 1.

Since the modeled landslide geometry is symmetrical with respect to the y axis, this fact is used to greatly reduce the size of the BEM discretization by only modeling half of the domain in the y direction and expressing a no-flow condition along the vertical (x, z) plane.

Landslide motion

We follow the wavemaker formalism proposed by Watts (1997,1998) and used in Grilli and Watts' (1999) 2D model, and extend it to 3D. Dimensional analysis shows that, within a family of similar landslide geometries, landslide motion and tsunami characteristics are functions of the five nondimensional independent variables : $\gamma = \rho_\ell/\rho_w$, θ, d/b, T/b, and $R = w/b$. Watts (1998) derived an approximate equation of motion describing the center of mass displacement of rigid underwater landslides, $S(t)$, parallel to the planar slope (in the negative x direction). For rigid landslides starting at rest at $t = 0$, we have,

$$S(t) = S_o\,\ln\left(\cosh\frac{t}{t_o}\right) \tag{22}$$

with,

$$S_o = \frac{u_t^2}{a_o} \quad ; \quad t_o = \frac{u_t}{a_o} \tag{23}$$

where a_o and u_t denote landslide initial acceleration and terminal velocity, respectively, given by,

$$a_o = g\,\frac{\gamma - 1}{\gamma + C_m}\,\sin\theta \tag{24}$$

where C_m is an approximate added mass coefficient, and,

$$u_t = \sqrt{gB}\,\sqrt{\frac{\pi(\gamma-1)}{2\,C_d}\,\sin\theta} \tag{25}$$

where C_d is an approximate drag coefficient. Watts (1997, 1998, 2000) found added mass and drag coefficients of $\mathcal{O}(1)$ for 2D and quasi-2D (where $W \gg B$) landslides. We have neglected Coulomb friction in our analysis.

The landslide geometry at time t is found from the initial geometry as,

$$\mathbf{x}_\ell(t) = \mathbf{x}_\ell(0) - S(t)\,(\mathbf{i}\cos\theta + \mathbf{k}\sin\theta) \tag{26}$$

where $\mathbf{i}$ and $\mathbf{k}$ denote unit vectors in the x and z directions, respectively. The center of mass velocity and acceleration at times $t > 0$ follow from,

$$\dot{S}(t) = u_t\,\tanh\frac{t}{t_o}\quad;\quad \ddot{S}(t) = a_o\left(\cosh\frac{t}{t_o}\right)^{-2} \tag{27}$$

Landslide velocity and acceleration at time t are easily found from Eq. (26) as,

$$\begin{aligned}\mathbf{u}_\ell &= -\dot{S}(t)\,(\mathbf{i}\cos\theta + \mathbf{k}\sin\theta)\\ \dot{\mathbf{u}}_\ell &= -\ddot{S}(t)\,(\mathbf{i}\cos\theta + \mathbf{k}\sin\theta)\end{aligned} \tag{28}$$

These can be used to define bottom boundary conditions (6) and (14).

Fig. 3 shows variations of $S(t)$, $\dot{S}(t)$ and $\ddot{S}(t)$ in nondimensional form, based on the above equations. Because this landslide displacement leads to an impulsive initial acceleration, a ramp-up of the acceleration from 0 to a_o, in the form of a tanh function, was added to the landslide kinematics model, over a small time $t_o/20$. Also, due to the finite length of the plane slope in the NWT, the landslide is sharply decelerated at some point in order for the landslide extremity to smoothly reach the slope bottom (at $x = x_o + d_o$) with both a zero speed and acceleration. Equations for the velocity and displacement were modified accordingly (see details in Watts *et al.*, 2001b). This led to more accurate numerical results in the NWT and also to a closer approximaiton of experimental measurements (see next section). Curves in Fig. 3 reflect this modification.

APPLICATIONS

Validation of snake AP boundary

The new absorbing piston (AP) boundary is validated by propagating a fully nonlinear solitary wave over constant depth h_o in the 3D-NWT. The initial wave height is $0.3h_o$ and the wave shape, potential and normal velocity are specified on the free surface based on Tanaka's (1986) method. The NWT is $15h_o$ long and discretized with 20 elements over x, 4 over y and 4 over z. One AP boundary is initially located at the far extremity at $x' = x/h_o = 15$. Due to the 2D geometry and boundary conditions, the AP boundary behaves here as a simple planar piston (within at least 6 significant figures). Fig. 4 shows vertical cross-sections at $y = 0$ in surface elevation calculated at various times. It is clear that most of the solitary wave leaves the NWT with only small surface perturbations left behind, thus demonstrating the efficiency of the AP boundary in eliminating wave reflection.

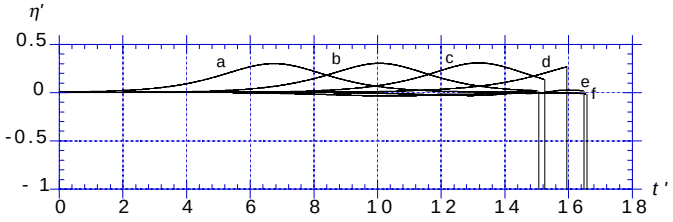

Fig. 4 : Dimensionless solitary wave elevation $\eta' = \eta/h_o$ as a function of $x' = x/h_o$ computed at dimensionless time $t' = t\sqrt{g/h_o}$= a: 0; b: 2.9; c: 5.6; d: 8.3; e:11.5; f: 14.9.

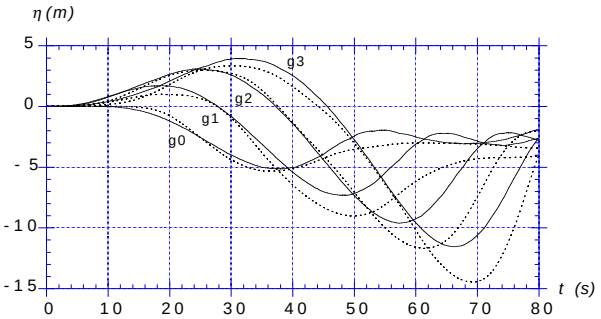

Fig. 5 : Landslide tsunami elevations calculated at numerical wave gages g0-g3 (——), as compared to laboratory measurements (- - - - -), for a quasi-2D case with : $\theta = 15°$, $\gamma = 1.81$, $C_m = 1.76$, $C_d = 1.53$, $B = 1{,}000$ m, $T = 52$ m, $d = 261$ m. Gages are on the x axis at x = g0 : 3,025.2 m; g1 : 2,725.2 m; g2 : 2,425.2 m; g3 : 2,125.2 m. Experimental results represent the smoothed average of three replicates of identical experiments.

Quasi-2D landslide tsunami simulation

For sake of comparison with earlier 2D results and with recent experimental results (Watts *et al.*, 2001a,b), the first landslide application presented here is a quasi-2D case in which we assume $W \ll B$ and, hence, do not specify a lateral (y) variation in landslide geometry. Therefore, we model the equivalent of a 2D slice along a uniform landslide in the 3D-NWT.

We assume the following landslide characteristics : a

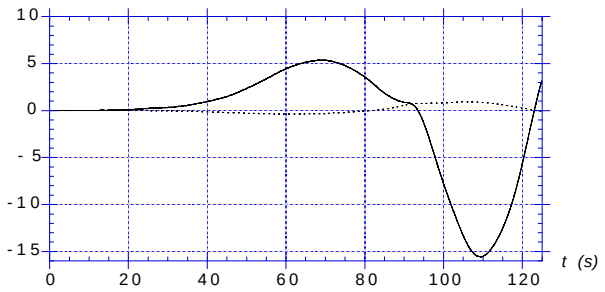

Fig. 6 : Same case as Fig. 5. Mean elevation $\overline{\eta}$ (——) and mean piston velocity $\overline{u_{ap}}$ (- - - - -) computed at the offhore absorbing piston boundary on $\Gamma_{r1}(t)$. Note the discontinuity in surface elevation around $t = 90$ s corresponding to the start of the sharp landslide deceleration in Fig. 3.

slope angle $\theta = 15°$, a rigid landslide with average density $\rho_\ell = 1,860$ kg/m^3 and thus $\gamma = 1.806$ for $\rho_w = 1,030$ kg/m^3, length $B = 1,000$ m and maximum thickness $T = 52$ m with no lateral variation, and initial submergence $d = 261$ m. This case was also modeled in the laboratory experiments of Watts *et al.* (2000, 2001b), at a 1:1000 scale. The landslide model was equipped with an accelerometer, which measured the model acceleration parallel to planar motion. Integrating the acceleration twice gave displacement as a function of time. A curve fit of displacement yielded initial acceleration a_o (following the observed ramp-up) and terminal velocity u_t from Eqs. (22) and (23). The added mass and drag coefficients were found to be $C_m = 1.76$, $C_d = 1.53$ from Eqs. (24) and (25), respectively. With these data, the landslide kinematics are quite close to those sketched in Fig. 3, with : $S_o = 3,673$ m, $u_t = 45.91$ m/s, $a_o = 0.574$ m/s^2, and $t_o = 80.00$ s (at prototype scale).

The initial domain length in the NWT was selected equal to one approximate tsunami wavelength, $\lambda = l_o + l_1 \simeq t_o\sqrt{g\,d} = 4,051.0$ m (Fig. 2), as estimated by Grilli and Watts (1999) based on theoretical scaling considerations. Laboratory experiments were performed on a plane surface piercing slope, i.e., without the shelf seen in Fig. 2. The shelf in the NWT was assumed shallow, with $h_1 = 0.075 h_o$, and to have an initial length l_1 such that the water volume above the shelf be identical to that of the same triangular section at the top of the slope in the experiments, i.e., $l_1 = h_1/(2\tan\theta)$. With $x_o = 0$ and $d_o = 400$ m, we find with this data : $h_o = 1,018.26$ m, $h_1 = 76.37$ m, $l_o = 3,751.0$ m, $l_1 = 135.9$ m, $x_\ell = 3,025.2$ m, and $x_i = 3,038.7$ m. In the experiments, the landslide geometry had elliptical cross-sections. In the following results, we used $\varepsilon = 0.5$ (and thus $b = 1,299$ m), which produces fairly narrow landslide cross-sections.

We specify 40 BEM elements in the x direction, of initial length $\Delta x_o = 101.28$ m, 4 elements in the half-width y direction (the minimum required number in the 3D-NWT), of length $\Delta y_o = 100$ m, and 6 elements over the depth. To better simulate experiments for this quasi-2D case, only one absorbing snake piston boundary is specified in the NWT, at the offshore extremity in the x-direction; the onshore vertical boundary is assumed impermeable. [Computations performed with a second absorbing boundary led to introducing water into the NWT through the onshore boundary, and to a corresponding increase in water level in the NWT. This may be more physical for actual landslides but does not simulate so well laboratory experiments. See Watts *et al.* (2001b) for details.] For a Courant number of 0.45, the initial time step is set to $\Delta t_o = 0.45\,\Delta x_o/\sqrt{g\,h_o} = 0.456$ s. The total number of nodes is 1,054 and there are 848 elements. With these inputs, the CPU time per time step is 3'44" on a Mac G4-450MHz.

Numerical wave gages were located in the NWT, 300 m apart along the x axis, at $x = 2,125.2$, 2,425.2, 2,725.2, and 3,025.2 m. Water elevations calculated at these gages are plotted in Fig. 5, as a function of time, and compared to the scaled-up experimental results. The agreement is quite good, considering the differences in landslide shape and motion, other effects such as sidewall friction and surface tension, and uncertainty on gage location, that occur in the experiments but not in the NWT. The characteristic tsunami amplitude for this case, in the sense of Grilli and Watts (1999), Watts *et al.* (2000, 2001a), is the maximum depression at gage g0, i.e., $|\,\eta_{\max}\,| = 5.16$ m in the NWT and 5.38 m in the scaled up experiments.

During these computations, the maximum cumulative error for the domain volume was 0.042%, and the maximum instantaneous error for the dimensionless continuity equation was 0.033%. The maximum error on theoretical landslide volume, due to discretization effects and landslide motion, was 0.40%. It was verified that all of these errors decreased when the size of the discretized elements also decreased. Results at BEM nodes with different y locations were found identical to within at least 6 significant figures, which is expected due to the two-dimensionality of the problem. This is also the case for the motion of the snake absorbing piston boundary, which behaves as a planar piston here, as during validation. Surface elevation and piston velocity for the AP boundary are given in Fig. 6 over a time representing $1.56 t_o$. A wave of elevation 5.31 m tall first leaves the NWT through $\Gamma_{r1}(t)$, at $t = 68.9$ s, and is later followed by a wave of depresion 15.57 m deep. The piston velocity goes from negative to positive and then negative again, i.e., piston motions are directed away from shore in the early part of the propagation.

Three-dimensional landslide

The second application presented here deals with a landslide of similar parameters but, this time, there is a lateral y variation in the landslide geometry. Hence, a full 3D landslide geometry is modeled using Eqs. (16) through (21), such as shown in Figs. 1 and 2. The landslide parameters are : a slope angle $\theta = 15°$, a rigid landslide with average density $\rho_\ell = 1,900$ kg/m^3 and thus $\gamma = 1.845$ for $\rho_w = 1,030$ kg/m^3, a length $B = 1,000$ m, width $W = 1,168$ m, maximum thickness $T = 103$ m, and initial submergence $d = 156$

m. The initial domain length is $l_o + l_1 = 2,500$ m (Figs. 1,2), with a shallow shelf of depth $h_1 = 0.115 h_o$ and initial length $l_1 = 200$ m at the extremity. With $x_o = 0$ and $d_o = 200$ m, we find with this data (Fig. 2) : $h_o = 635.81$ m, $h_1 = 73.12$ m, $x_\ell = 1,592.7$ m, and $x_i = 1,619.38$ m. We use $\varepsilon = 0.25$ (and thus $b = 1,317$ m), which does produce fairly narrow landslide cross-sections. Two AP boundaries are used at both extremities of the NWT in the x direction, which this time behave as snake boundaries due to 3D effects. Lateral boundaries are kept impermeable, but are located sufficiently far from the landslide, at a distance $y = \pm 1,800$ m (i.e., the NWT width is 3,600 m), to allow for a sufficient time of computation before lateral wave reflections affect results at the numerical wave gages.

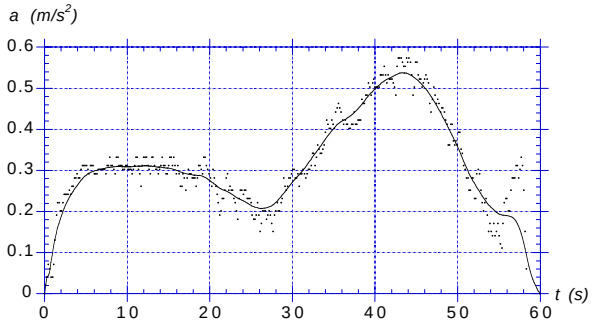

Fig. 7 : Measured (•) and smoothed (——) acceleration for a 3D semi-ellipsoidal landslide model, as a function of prototype time (Watts *et al.*, 2001b). With : $\theta = 15°$, $\rho_\ell = 1,900$ kg/m^3, $B = 1,000$ m, $W = 1,168$ m, $T = 103$ m, $d = 156$ m. [Model to prototype length scale is 1:1000 and time scale is 1:31.62]

We specify 40 BEM elements in the x direction, of initial length $\Delta x_o = 62.5$ m, 11 elements in the half-width y direction, of length $\Delta y_o = 163.64$ m, and 6 elements over the depth. For a Courant number of 0.5, the initial time step is set to $\Delta t_o = 0.5\, \Delta x_o / \sqrt{g\, h_o} = 0.40$ s. The total number of nodes for the half-width domain is 1,726 and there are 1,492 elements. With these inputs, the CPU time per time step is 14'30" on a Mac G4-450MHz. The landslide geometry and NWT bottom discretization are shown in Fig. 1.

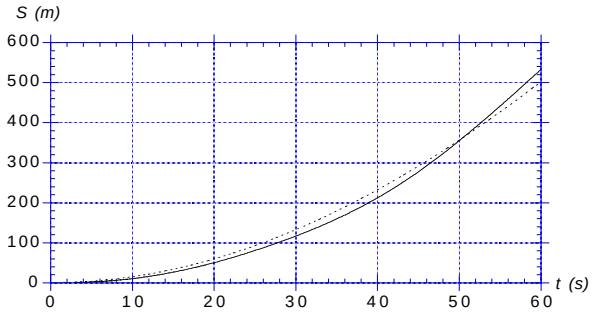

Fig. 8 : Same case as Fig. 7. Measured (——) and curve fitted (- - - - -) (with Eq. (22)) motion for 3D semi-ellipsoidal landslide model, as a function of prototype time.

Watts *et al.* (2001b) also conducted laboratory experiments, at 1:1000 scale, for a 3D semi-ellipsoidal model of a rigid underwater landslide sliding down a planar 15° slope. As in the previous quasi-2D case, the landslide acceleration measured during the experiments is used to derive the parameters of the landslide kinematics specified in the NWT. These experiments had 12 wave gages instead of four, thereby deferring a comparison between experimental and numerical results to another paper with more space (Watts *et al.*, 2001b). Fig. 7 shows the measured landslide acceleration $a(t)$, and Fig. 8 the landslide motion $S(t)$ obtained by integrating the acceleration twice with respect to time. The best fit of Eq. (22) to the measured motion (Fig. 8) results in $S_o = 2,269$ m and $t_o = 86.96$ s (at prototype scale). Applying Eqs. (23) through (25) to these results, we further find $a_o = 0.3$ m/s^2, which is consistent with the measurements in Fig. 7, and $u_t = 26.09$ m/s although this velocity may not be reached in practice. These parameters are used to specify the landslide kinematics in the NWT, using Eqs. (22) to (28).

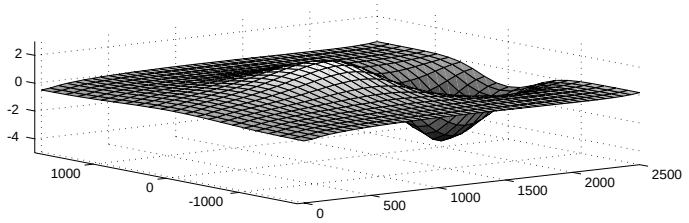

Fig. 9 : Same case as Figs. 7-8. Surface elevation (in meters) for a 3D tsunami landslide calculated in the NWT, at $t = 19.1$ s. With : $\gamma = 1.845$, $a_o = 0.3$ m/s^2, $u_t = 26.09$ m/s, and $\varepsilon = 0.25$.

Fig. 9 shows the free surface computed at $t = 19.1$ s. We clearly see a wave of elevation followed by a wave of depression initially propagating offshore. Three-dimensional energy spreading is also clearly seen on the figure. Figs. 10 and 11 show wave elevations computed at a few of the 12 numerical wave gages as a function of time. The three-dimensionality and spreading of the tsunami is apparent from the gage records. More details of results and comparisons with experiments can be found in Watts *et al.* (2001b).

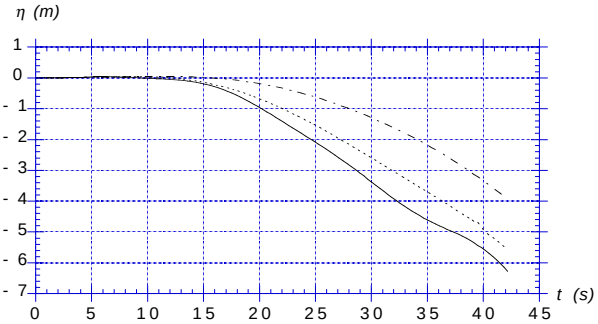

Fig. 10 : Same case as Figs. 7-11. Surface elevation for a 3D tsunami landslide calculated in the NWT, at gages located at $(x, y) = (1592.7,0)$ (——-); (1592.7,300) (- - - - -); (1592.7,600).

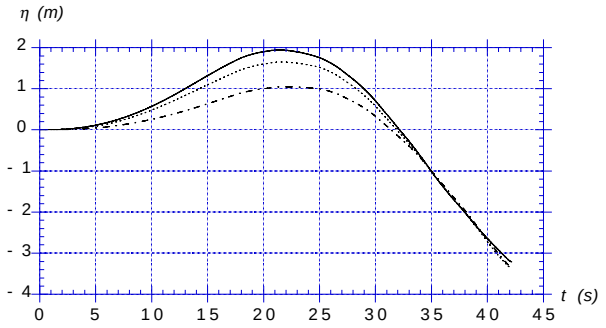

Fig. 11 : Same case as Figs. 7-11. Surface elevation for a 3D tsunami landslide calculated in the NWT, at gages located at (x, y) = (992.7,0) (——-); (992.7,300) (- - - - -); (992.7,600).

During these computations, the maximum cumulative error for the domain volume was 0.039%, and the maximum instantaneous error for the dimensionless continuity equation was 0.0055%. The maximum error on theoretical landslide volume, due to discretization effects and landslide motion, was 0.10%. Looking at results for gages farther away from the landslide and closer to the offshore AP boundary (Figs. 11), it is clear that little reflection occurs at the open boundary.

CONCLUSIONS

Landslide tsunami generation mechanisms were explored using a three-dimensional Numerical Wave Tank (NWT) solving fully nonlinear potential flow theory. New features were added to the NWT (model of underwater landslide geometry and motion, snake absorbing piston boundaries) and their accuracy and efficiency was tested for certain applications. Two landslide cases are presented here and results of the first one, a quasi-2D landslide, are validated using experimental results. The second case deals with a fully 3D landslide and shows realistic results during tsunami generation. To our knowledge, results based on fully nonlinear 3D wave computations have never been reported for a landslide tsunami source. Such a wave field can be used as an initial condition in long wave based tsunami propagation and runup models.

REFERENCES

Brandini, C. and S.T. Grilli (2001). "Modeling of freak wave generation in a 3D-NWT," *Proc. ISOPE 2001 Symp.* (Stavenger, Norway, June 2001), 8 pps.

Clément, A. (1996). "Coupling of two absorbing boundary conditions for 2D time-domain simulations of free surface gravity waves," *J. Comp. Phys.*, Vol 26, pp 139-151.

Fryer, G.J., Watts, P., Pratson, L.F. and J.V. Gardner (2001). "The tsunami of 1 April 1946: A landslide in the upper forearc," *in Prediction of Underwater Landslide Hazards,* Balkema Press, Rotterdam.

Grilli, S.T., Guyenne, P. and F. Dias (2000). "Modeling of overturning waves over arbitrary bottom in a 3D numerical wave tank," *Proc. 10th Offshore and Polar Engng. Conf.* (ISOPE00, Seattle, USA, May 2000), ISOPE, Vol III, pp 221-228.

Grilli, S.T., Guyenne, P. and F. Dias (2001). "A fully nonlinear model for three-dimensional overturning waves over arbitrary bottom," *Intl. J. Numer. Methods in Fluids*, Vol 34, 39 pps (in press).

Grilli, S.T. and J. Horrillo (1997). "Numerical generation and absorption of fully nonlinear periodic waves," *J. Engng. Mech.*, Vol 123(10), pp 1060-1069.

Grilli, S.T. and P. Watts (1999). "Modeling of waves generated by a moving submerged body. Applications to underwater landslides." *Engng. Analysis Boundary Element,* Vol 23, pp 645-656.

Murty, T.S. (1979). "Submarine slide-generated water waves in Kitimat Inlet, British Columbia," *J. Geoph. Res.,* Vol 84(C12), pp 7777-7779.

Tanaka, M. (1986). "The stability of solitary waves," *Phys. Fluids,* Vol 29(3), pp 650-655.

Tappin, D.R., Matsumoto, T. and Shipboard Scientists (1999). "Offshore surveys identify sediment slump as likely cause of devastating Papua New Guinea tsunami 1998," *Eos,* Vol 80(30), p 329.

Tappin, D.R., Watts, P., McMurtry, G.M., Lafoy, Y. and T. Matsumoto (2001). "The Sissano, Papua New Guinea tsunami of July 1998 – Offshore evidence on the source mechanism," *Marine Geology,* (in press).

Watts, P. (1997). "Water waves generated by underwater landslides," *PhD thesis*, California Inst. of Technol., Pasadena, CA.

Watts, P. (1998). "Wavemaker curves for tsunamis generated by underwater landslides," *J. Wtrwy, Port, Coast, and Oc. Engrg.,*" Vol 124(3), pp 127-137.

Watts, P. (2000). "Tsunami features of solid block underwater landslides." *J. Waterways, Port, Coastal and Ocean Engng.,* Vol 126(3), pp 144-152.

Watts, P., Imamura, F. and S.T. Grilli (2000). "Comparing model simulations of three benchmark tsunami generation cases," *J. Science Tsunami Hazards*, Vol 18(2), pp 107-123.

Watts, P., Grilli, S.T. and C.E. Synolakis (2001a). "Tsunami generation by submarine mass failure. I: Wavemaker models," *J. Wtrwy, Port, Coast, and Oc. Engrg.* (to be submitted).

Watts, P., Grilli, S.T. and A. Bengston (2001b). "Experimental validation of landslide tsunami simulation in a 3D numerical wave tank," (in preparation).